Robust Tracking Control of a Prosthesis Test Robot

Hanz Richter
Associate Professor
Mechanical Engineering Department,
Cleveland State University,
Cleveland, OH 44115
e-mail: h.richter@csuohio.edu

Dan Simon
Professor
Electrical and Computer Engineering Department,
Cleveland State University,
Cleveland, OH 44115
e-mail: d.j.simon@csuohio.edu

This paper develops a passivity-based robust motion controller for a robot used in prosthetic leg performance studies. The mathematical model of the robot and passive prosthesis corresponds to a three degree-of-freedom, underactuated rigid manipulator. A form of robotic testing of prostheses involves tracking reference trajectories obtained from human gait studies. The robot presented in this paper emulates hip vertical displacement and thigh swing, and we consider a prosthesis with a passive knee for control development. The control objectives are to track commanded hip displacements and thigh angles accurately, even in the presence of parametric uncertainties and large disturbance forces arising from ground contact during the stance phase. We develop a passivity-based controller suitable for an underactuated system and compare it with a simple independent-joint sliding mode controller (IJ-SMC). This paper describes the mathematical model and nominal parameters, derives the passivity-based controller using Lyapunov techniques and reports success in real-time implementation of both controllers, whose advantages and drawbacks are compared. [DOI: 10.1115/1.4026342]

1 Introduction

The development of novel prosthetic devices has progressed at a rapid pace in the last decades. Transfemoral leg prostheses, in particular, have become increasingly sophisticated in terms of the technologies used to modulate knee behavior or even produce push-off forces with battery power. Knee torque may be varied by pneumatic, hydraulic, or fluid-rheological means, and embedded microprocessors are typically used for control [1]. Much research effort continues to be focused on the design and control of prostheses capable of fully restoring normal gait [2–6]. Robotic testing is a viable method to evaluate and compare prosthesis prototypes without clearance burdens and with improved repeatability in comparison with human trials. Moreover, a machine may be fitted with sensors which would be inadequate or difficult to install in a patient. Robotic testing has the potential to accelerate the development of new prosthesis concepts, as new hardware and control ideas can be examined in safe and controlled conditions. Some use of commercial manufacturing robots in prosthesis testing has been reported by the Fraunhofer Institute [7] and the Cleveland Clinic [8]. This paper is concerned with a recently developed robot [9,10] designed for transfemoral prosthesis tests using hip vertical displacement and thigh angle as input trajectories. These two degrees of freedom are the minimum necessary to emulate human walking in the sagittal plane. The overall robot configuration depends on the type of prosthesis attached to the machine interface plate. When a passive prosthesis for transfemoral amputees is installed, the overall system can be modeled as a three-link rigid robot with one underactuated joint (i.e., the knee joint) with damping. As shown in Fig. 1, the machine's vertical axis is fixed, and walking is emulated using a treadmill. When a test is conducted, hip displacement and thigh angle histories measured from normal human gait are used as reference commands to the robot's actuated degrees of freedom. Variables, such as knee angle, ground reaction force, and hip torque are either measured directly or calculated from the measurements using models of the prosthesis and the machine. It is thus imperative for the controller to achieve accurate trajectory tracking in the presence of parametric uncertainty and modeling error associated with machine and prosthesis. Moreover, this paper considers the control objective to be pure trajectory control, even during periods of contact with the treadmill, where large forces applied to the foot are generated. Thus, ground reaction is regarded as an external disturbance to be accommodated by the controller. Since the prosthetic foot and the treadmill belt are compliant, the user may adjust the peak value of ground reaction force by lowering the center of oscillation of hip displacement. Note that hybrid force-position control [11,12] and impedance control [13] are also possible with this equipment.

A robust control approach is mandatory, given that key dynamic parameters, such as some masses, moments of inertia, center-of-mass locations, and friction are subject to significant measurement errors. The robot controller should also require little or no modification when different (passive) prostheses are installed or when the reference trajectories are changed. This paper develops a coupled controller following the passivity-based robotic control technique, suitably extended to account for underactuation and external disturbance. This design is presented in contrast with an independent-joint (decoupled) sliding mode controller which is based on actuator models only.

The paper is organized as follows: Section 2 describes machine functionality and components and presents the mathematical model and its structural properties; Sec. 3 derives the passivity-based controller, proving uniform ultimate boundedness of the tracking error; Sec. 4 presents the independent-joint sliding mode controller; Sec. 5 reports the real-time control results, and Sec. 6 offers conclusions and recommendations for further development.

2 Test Robot Description

A schematic diagram of the robot and its components and a photograph of the robot with a prosthesis and flexible foot are shown in Fig. 1. Vertical motion is generated by a linear slide driven by a ballscrew with a pitch of 12.7 mm/rev. A brushless dc motor (Mitsubishi HF-KP73) is directly coupled to the ballscrew. The motor is powered by a torque-mode servo amplifier (Mitsubishi MR-J3-70A). An analog input voltage applied to the servo amplifier results in a proportional torque on the motor shaft and ballscrew. Vertical position (hip displacement) is measured with an incremental encoder rotating synchronously with the motor. An absolute position reference is established with a limit switch mounted on the vertical guides. The total useful travel of the slide is 12 in. The rotary motion stage, including motor, is carried by the vertical slide. The rotary servo system is composed of a brushless dc motor (ElectroCraft RapidPower RP34) coupled to a rotary plate through an inchworm-gear reducer with ratio 80:1. Angular position (thigh angle) is measured with an incremental encoder

Contributed by the Dynamic Systems Division of ASME for publication in the Journal of Dynamic Systems, Measurement, and Control. Manuscript received February 1, 2013; final manuscript received December 1, 2013; published online February 19, 2014. Assoc. Editor: Won-jong Kim.

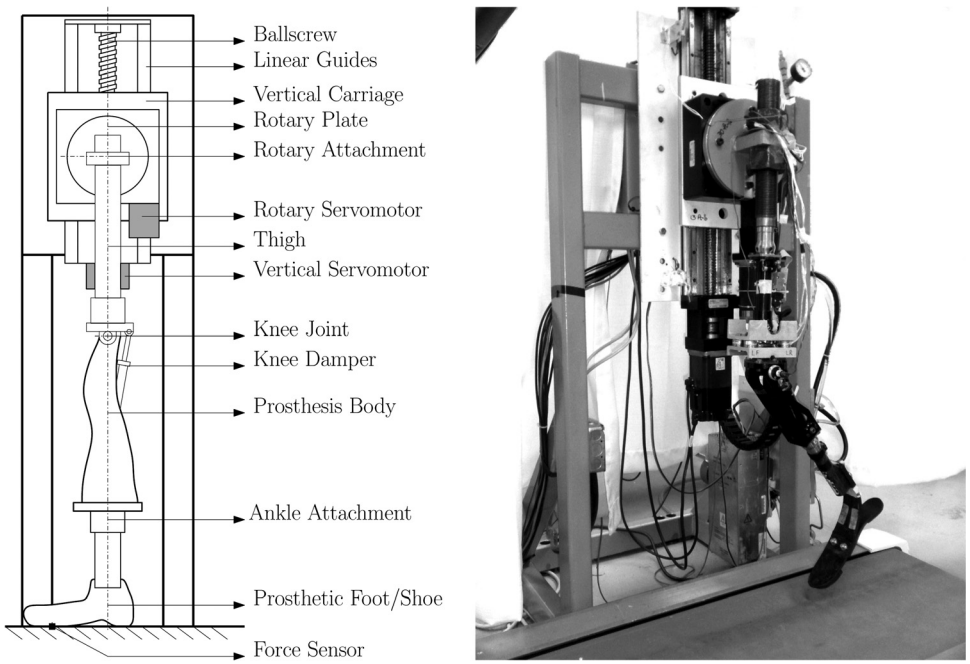

Fig. 1 Machine schematic and overall robot installation

rotating synchronously with the motor. An absolute position reference is established with a limit switch mounted on the rotary plate. Prostheses are attached to the rotary plate by means of an adjustable threaded rod, which is secured to a bracket on the plate with two 2.75-in. nuts. The threaded rod, in combination with the adjustable center of oscillation of the vertical stage, offers flexibility for standoff adjustments. Although thigh angular excursion in the normal gait data does not exceed 50 deg, the rotary actuator has an unlimited angular range. The linear slide is attached to a rigid steel frame. The prosthesis used for proof-of-concept tests with the robot is the Mauch MicroLite S [14], which consists of two rigid links connected by a rotary joint. A damper is connected between the links, as shown in Fig. 1, to stabilize the knee during the stance phase and limit knee angle during the swing phase. The flexible prosthetic foot is fitted with a strain gage calibrated to measure the vertical component of ground reaction force. A treadmill is secured to the frame, and anchor bolts are used to secure the entire assembly to the lab floor. Normal gait profiles used as a guideline for design are a subset of the data collected by van den Bogert [15], which includes walking and running in healthy subjects. The machine is designed for hip displacement amplitudes of up to 50 mm with a maximum velocity of 1 m/s. Vertical force capacity is specified at 1200 N, which exceeds the ground force generated by a 78 kg normal subject during fast walking or slow running. Real-time instrumentation and control is handled by a dSPACE DS-1102 system and associated software.

2.1 Mathematical Model. The overall machine-and-prosthesis system has been modeled in the standard framework of robotics [16]. When a passive leg prosthesis is attached, the system is underactuated, since the torque of the knee joint cannot be externally controlled. Knee damping for the Mauch MicroLite S knee may be manually set to two separate constant values for flexion and extension using the prosthesis' adjustment rings, however. When advanced prototypes featuring actively controlled damping or powered knee actuation are attached, the system can be regarded as semi-actuated or fully actuated. A forward kinematics model is available [9,10], which allows the computation of the position and velocity of any point given the positions and velocities of the joints. For the purposes of this paper, the point of application of the vertical ground reaction and its corresponding Jacobian are of interest. These quantities have been listed in the Appendix. Figure 2 shows the coordinate frames used in the kinematic model, where l_2 is the length of link 2 (thigh), d_0 is the

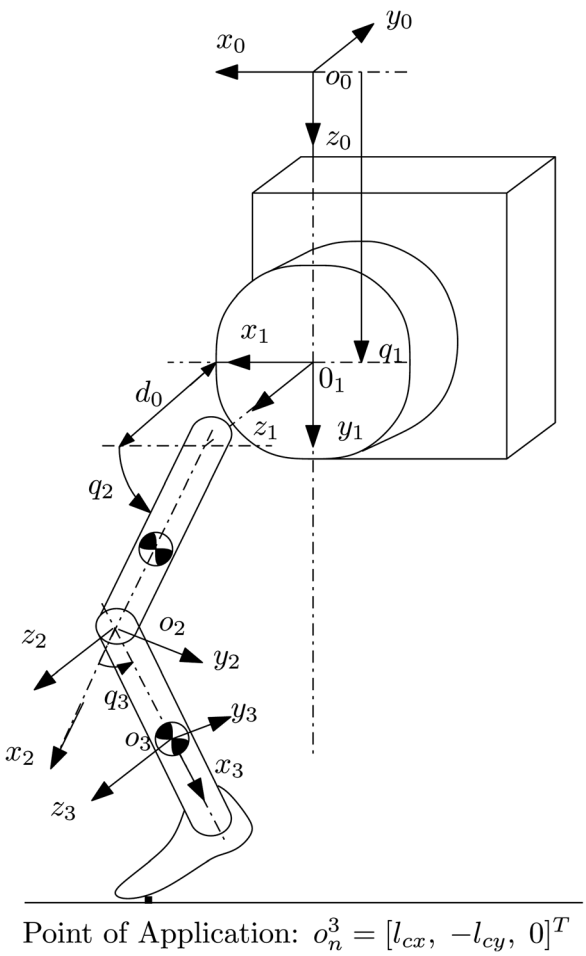

Fig. 2 Denavit–Hartenberg coordinate frame assignments

offset of link 2, and c_3 is the distance between the knee joint and the center of mass of link 3. Frame assignments follow the Denavit–Hartenberg convention [17]. The world-frame coordinates of points of interest can be readily computed assuming the joint coordinate vector q is known. In frame 3 coordinates, ground reaction is applied at $[l_{cx} - l_{cy}0]^T$. The vertical coordinate Z_{LC} of the point of application can be found using the composite transformation from frame 3 to the world frame (see Appendix). The dynamic model for the robot and passive prosthesis is given in joint coordinates as

$$M(q)\ddot{q} + C(q,\dot{q})\dot{q} + B\dot{q} + N(q,\dot{q}) + g(q) + F_f + J_e^T F_e = \begin{bmatrix} K_a u_a \\ 0 \end{bmatrix} \tag{1}$$

where $q^T = [q_1\ q_2\ q_3]$ is the vector of joint displacements (in our case q_1 is the hip vertical displacement, q_2 is the thigh angle, and q_3 is the knee angle), u_a is the vector of control inputs, $M(q)$ is the mass matrix, $C(q,\dot{q})$ is a matrix accounting for centripetal and Coriolis effects, $N(q,\dot{q})$ is a nonlinear damping matrix (in our case due to the knee damper), B is a viscous damping matrix, F_f is a vector of Coulomb friction terms, J_e is the kinematic Jacobian relative to the point of application of external forces F_e, $g(q)$ is the gravity vector, and K_a is a diagonal matrix of actuator gains. The explicit entries of the above matrices are found in Refs. [9,10], and their regressor form is listed in the Appendix. Note that actuator dynamics can be considered in this model by adding reflected actuator inertias (i.e., weighted by the square of gear ratio) in the entries of M. Viscous damping is significant only in the rotary mechanism, with coefficient b. Coulomb friction of magnitude f is considered only for the vertical slide, where it is significant. The nonlinear damping term $N(q,\dot{q})$ corresponds to a Rayleigh dissipation function for the knee damper [9,10]. We decompose the vector of joint coordinates into actuated and unactuated components as $q^T = [q_a^T\ q_u^T]$. The friction terms are decomposed along actuated and unactuated coordinates as $F_f^T = [F_{fa}^T\ 0]$, $(B\dot{q})^T = [(B_a\dot{q}_a)^T 0]$ and $N^T = [0\ R(q_3,\dot{q}_3)]$, with $B_a = \mathrm{diag}([0\ b])$ and $F_{fa}^T = [f\,\mathrm{sign}(\dot{q}_1)0]$.

The prosthesis is regarded as links 2 and 3 of the overall robot. Joint 3 is subject to an internal torque due to damper action. This nonlinear damping torque can be calculated as $\partial\mathcal{R}/\partial\dot{x}_d$, where $\mathcal{R}$ is the Rayleigh dissipation function

$$\mathcal{R} = \frac{1}{2} b_k \dot{x}_d^2 \tag{2}$$

where b_k is a direction-dependent damping coefficient and $\dot{x}_d$ is the expansion rate of the damper. The expansion rate is readily found by considering the geometry of the damper attachment and using differentiation of the cosine law. The nonlinear damping term of Eq. (1) is thus found to be

$$R(q_3,\dot{q}_3) = -\frac{b_k o_d^2 r_d^2 \cos^2(q_3)\dot{q}_3}{l_d^2} \tag{3}$$

where o_d, r_d, and l_d are the damper offset, swing radius, and instantaneous damper length, as shown in Fig. 3. It is important to note that the external force Jacobian J_e contains only link lengths as parameters. Since lengths can be measured with very small errors and the vertical component of ground reaction F_e is measured in real-time, the term $J_e^T F_e$ can be regarded as a measurable disturbance that can be compensated directly by the real-time controller. Partition this term along actuated and unactuated coordinates as $J_e^T F_e = [F_a^T | F_u]^T$ and define a control input w_a as

$$w_a = K_a u_a - F_a \tag{4}$$

The horizontal component of ground reaction is not measured in the real-time system and is difficult to describe without an ankle/foot model. However, it is anticipated to have a small effect on thigh rotation due to the high gear ratio used in the mechanism. It is not considered for the theoretical derivation. The model of Eq. (1) is now partitioned into actuated and unactuated coordinates as

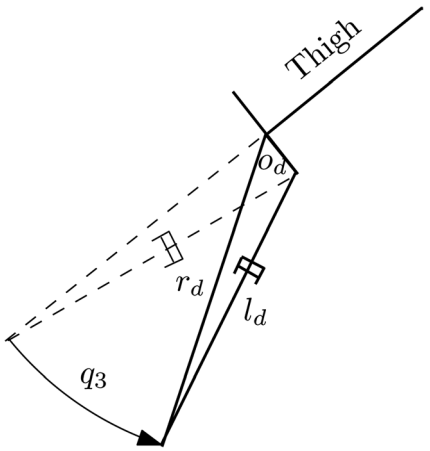

Fig. 3 Damping cylinder and knee geometry. The indicated direction for q_3 is positive (flexion), the opposite is extension. The cylinder has separate adjustment rings for the damping coefficient during flexion and extension.

$$M_{11}\ddot{q}_a + M_{12}\ddot{q}_u + C_{11}\dot{q}_a + C_{12}\dot{q}_u + B_a\dot{q}_a + g_a + F_{fa} = w_a \tag{5}$$

$$M_{21}\ddot{q}_a + M_{22}\ddot{q}_u + C_{21}\dot{q}_a + C_{22}\dot{q}_u + R(\dot{q}_u, q_u) + g_u + F_u = 0 \tag{6}$$

where the dependence of M, C, F_{fa}, g_a, and g_u on the joint coordinates and their velocities has been omitted from the notation.

2.2 Structural Properties. We note that the well-known properties of *skew symmetry*, *linearity in the parameters*, and *inertia matrix boundedness* apply to the above partitioned model as shown next. The model of Eq. (1) satisfies the property that $\dot{M}(q) - 2C(q,\dot{q})$ is a skew-symmetric matrix. Clearly, the property also applies to the block-diagonal elements of any partition of $M(q)$ and $C(q,\dot{q})$. In particular, $\dot{M}_{11} - 2C_{11}$ must be skew symmetric.

The linearity-in-parameters property states that $M(q)\ddot{q} + C(\dot{q},q)\dot{q} + g(q)$ can always be factored as $Y(\ddot{q},\dot{q},q)\Theta$, where the *regressor matrix* Y does not contain any physical or dimensional constants [16]. All such constants appear in combination as a set of parameters forming the entries of a *parameter vector* Θ. A minimal set of parameters exists for each kinematic configuration, and their determination must be done by algebraic manipulation on a case-by-case basis. We note that the linear parameterization property is applicable to a partitioned model. Furthermore, when Coulomb friction and linear viscous damping terms are present, it is still possible to obtain a linear parameterization. For the robot and passive prosthesis, the minimal parameterization leads to a regressor Y with three rows and nine columns (parameters). As elaborated below, Eq. (5) is partitioned again along each actuated coordinate to facilitate tuning of certain control gains. This operation yields the set of regressors and corresponding parameters shown in the Appendix.

The inertia matrix boundedness property guarantees that there exist constants $\bar{\rho}_M$ and $\underline{\rho}_M$ such that $\underline{\rho}_M \leq \| M \| \leq \bar{\rho}_M$, where any suitable norm may be used. Evidently, the block entries of a partition of M must also possess absolute upper and lower bounds. This property will be used below to guarantee that the knee acceleration estimation error term will not cause a Lyapunov derivative to be positive.

3 Robust Passivity-Based Controller

The following development follows the framework of passivity-based control [16]. Significant extensions to the standard case are required to handle underactuation, to compensate for friction and disturbance and to facilitate tuning. Suppose that the actuated joints must follow reference trajectories given by functions of time $q_a^d(t)$, while the unactuated joints must remain bounded. For this, define a function $s_a = \dot{q}_a - \dot{q}_a^d + \Lambda(q_a - q_a^d)$, where Λ is a positive-definite diagonal matrix. Note that this definition coincides with the notion of sliding function used in the sliding mode control of second-order systems. Thus, if s_a and its derivatives become zero, first-order decay dynamics will be obtained for the tracking error $\tilde{q}_a = q_a - q_a^d$. Defining $v_a = \dot{q}_a^d - \Lambda_a \tilde{q}_a$, we have

$$s_a = \dot{q}_a - v_a \tag{7}$$

$$\dot{s}_a = \ddot{q}_a - a_a \tag{8}$$

where $a_a = \dot{v}_a$. Define the Lyapunov function candidate

$$V_r = \frac{1}{2} s_a^T M_{11} s_a + \tilde{q}_a^T \Lambda (B_a + \Pi) \tilde{q}_a \tag{9}$$

where Π is a positive-definite diagonal matrix. The time derivative of V_r is given by

$$\dot{V}_r = s_a^T M_{11} \dot{s}_a + \frac{1}{2} s_a^T \dot{M}_{11} s_a + 2\tilde{q}_a^T \Lambda (B_e + \Pi) \dot{\tilde{q}}_a^T$$

The skew-symmetry property applied to M_{11} and C_{11} implies that

$$\dot{V}_r = s_a^T (M_{11} \dot{s}_a + C_{11} s_a) + 2\tilde{q}_a^T \Lambda (B_a + \Pi) \dot{\tilde{q}}_a^T$$

Using Eqs. (7) and (8) yields

$$\begin{aligned} \dot{V}_r = s_a^T (&-M_{11} a_a - C_{11} v_a - M_{12} \ddot{q}_u - C_{12} \dot{q}_u \\ &- B_a s_a - B_a v_a - g_a - F_{fa} + w_a) + 2\tilde{q}_a^T \Lambda (B_a + \Pi) \dot{\tilde{q}}_a^T \end{aligned}$$

To construct a control law, we assume that only the structure of the model matrices is known, but that the parameters are uncertain. However, we assume that parametric uncertainties are bounded. Also, we assume that joint positions and velocities are directly available, and that the acceleration of the unactuated joint is estimated (for instance through numerical differentiation), with a known estimation error bound. Therefore we postulate a control input of the form

$$\begin{aligned} w_a = &\hat{M}_{11} a_a + (\hat{C}_{11} + B_a) v_a + \hat{M}_{12} \hat{a}_u \\ &+ \hat{C}_{12} \dot{q}_u + \hat{g}_a + \hat{F}_{fa} - \Pi s_a + w_2 \end{aligned} \tag{10}$$

where the circumflex notation has been used to indicate estimated quantities. In particular, $\hat{a}_u$ is the estimated acceleration of the unactuated joints. Also, w_2 is an additional control term used to compensate for the acceleration estimation error, as shown below. The linear parameterization property establishes that there exist a regressor $Y(a_a, v_a, \hat{a}_a, \dot{q}_u, \dot{q}_u, q_a, q_u)$ and corresponding parameter vector Θ such that

$$\begin{aligned} &\hat{M}_{11} a_a + (\hat{C}_{11} + B_a) v_a + \hat{M}_{12} \hat{a}_u + \hat{C}_{12} \dot{q}_u + \hat{g}_a + \hat{F}_{fa} \\ &\quad = Y(a_a, v_a, \hat{a}_a, \dot{q}_u, \dot{q}_u, q_a, q_u) \hat{\Theta} \end{aligned}$$

To simplify control gain tuning, the above equation is partitioned again along the individual actuated joints. In the case of the leg prosthesis test robot, there are two actuated joints: hip vertical displacement and thigh angle. For this case, we thus consider the decomposition

$$w_a = \begin{bmatrix} Y_1 \hat{\Theta}_1 \\ Y_2 \hat{\Theta}_2 \end{bmatrix} - \Pi s_a + w_2 \tag{11}$$

where the arguments of the regressors have been omitted. Substituting Eq. (11) into the Lyapunov derivative yields

$$\begin{aligned} \dot{V}_r = &s_1 Y_1 (\hat{\Theta}_1 - \Theta_1) + s_2 Y_2 (\hat{\Theta}_2 - \Theta_2) - s_a^T (B_a + \Pi) s_a \\ &- s_a^T M_{12} \tilde{a}_u + s_a^T w_2 + 2\tilde{q}_a^T \Lambda (B_a + \Pi) \tilde{q}_a \end{aligned}$$

where $\tilde{a}_u = \ddot{q}_u - \hat{a}_u$ is the acceleration estimation error for the unactuated joint. In this robust control approach, we assume that only nominal values for the parameters are available, namely, Θ_{10} and Θ_{20}, where known bounds exist for their errors relative to the true parameters

$$\|\Theta_{10} - \Theta_1\| \le \rho_{11} \tag{12}$$

$$\|\Theta_{20} - \Theta_2\| \le \rho_{12} \tag{13}$$

The inertia matrix boundedness property implies that $\|M_{12}(q)\|$ is upper-bounded by a constant (see Appendix). Assuming that the unactuated acceleration is computed with some known maximum error, a norm bound can be established for the term $M_{12}\tilde{a}_u$

$$\|M_{12} \tilde{a}_u\| \le \rho_2 \tag{14}$$

Now choose $\hat{\Theta}_i = \Theta_{i0} + \Delta\Theta_i$ for $i = 1,2$, where $\Delta\Theta_i$ are new controls to be determined below. Substituting the definition of s_a into the term $s_a^T (B_a + \Pi) s_a$ and combining terms leaves the Lyapunov derivative in the form

$$\begin{aligned} \dot{V}_r = &s_1 Y_1 (\tilde{\Theta}_1 + \Delta\Theta_1) + s_2 Y_2 (\tilde{\Theta}_2 + \Delta\Theta_2) \\ &+ s_a^T (w_2 - M_{12} \tilde{a}_u) - e^T Q e \end{aligned} \tag{15}$$

where the error state has been defined as $e^T = [\tilde{q}_a^T | \dot{\tilde{q}}_a^T]$ and Q is a block-diagonal matrix with blocks $\Lambda(B_a + \Pi)\Lambda$ and $(B_a + \Pi)$.

Since Θ_i are norm-bounded, the terms $\Delta\Theta_i$ can be adjusted according to the switching feedback laws $\Delta\Theta_i = -\rho_{1i}(s_i Y_i / \|s_i Y_i\|)$ whenever $\|s_i Y_i\| \neq 0$, with $\Delta\Theta_i = 0$ otherwise. Indeed, the following inequality holds:

$$s_i Y_i (\tilde{\Theta}_i + \Delta\Theta_i) \le \|s_i Y_i\| \, \|\tilde{\Theta}_i\| - \rho_{1i} \|s_i Y_i\| \le 0$$

Similarly, since the $M_{12}\tilde{a}_u$ is norm-bounded, w_2 can be chosen as $-\rho_2(s_a / \|s_a\|)$ whenever $\|s_a\| \neq 0$ and $w_2 = 0$ otherwise. The following inequality holds:

$$-s_a^T M_{12} \tilde{a}_u - s_a^T \rho_2 \frac{s_a}{\|s_a\|} \le \|s_a\| \, \|M_{12} \tilde{a}_u\| - \rho_2 \|s_a\| \le 0$$

Since the term $-e^T Q e$ is negative-definite, the above choices render the Lyapunov derivative negative-definite.

These laws are of the *variable-structure* type and their switching action requires unlimited actuator bandwidth [18]. A continuous approximation of these laws is therefore adopted

$$\Delta\Theta_i = \begin{cases} -\rho_{1i} \dfrac{s_i Y_i^T}{\|s_i Y_i\|}, & \text{if} \quad \|s_i Y_i\| > \varepsilon_{1i} \\ -\rho_{1i} \dfrac{s_i Y_i^T}{\varepsilon_{1i}}, & \text{if} \quad \|s_i Y_i\| \le \varepsilon_{1i} \end{cases} \tag{16}$$

where $\varepsilon_{1i} > 0$ are small positive constants. Similarly, w_2 is chosen as

$$w_2 = \begin{cases} -\rho_2 \dfrac{s_a}{\|s_a\|}, & \text{if} \quad \|s_a\| > \varepsilon_2 \\ -\rho_2 \dfrac{s_a}{\varepsilon_2}, & \text{if} \quad \|s_a\| \le \varepsilon_2 \end{cases} \tag{17}$$

where ε_2 is a small positive constant. With this approximation, the closed-loop control system is guaranteed to possess the property of *uniform ultimate boundedness* [19] (uub) of the error trajectories. The guaranteed uub radius is estimated as follows: Assuming the "worst-case" where $\|s_i Y_i\| \le \varepsilon_{1i}$ and $\|s_a\| \le \varepsilon_2$ at the same time, the following inequality holds:

$$\begin{aligned} \dot{V}_r &= \sum_{i=1}^{2} s_i Y_i \left(\tilde{\Theta}_i - \rho_{1i} Y_i^T \frac{s_i}{\|s_i Y_i\|} \Theta_i \right) \\ &\quad + s_a \left(-M_{12} \tilde{a}_u - \rho_2 \frac{s_a}{\|s_a\|} \right) - e^T Q e \\ &\le \sum_{i=1}^{2} \|s_i Y_i\| \rho_{1i} \left(1 - \frac{\|s_i Y_i\|}{\varepsilon_{1i}} \right) + \|s_a\| \rho_2 \left(1 - \frac{\|s_a\|}{\varepsilon_2} \right) - e^T Q e \end{aligned}$$

which reduces to

$$\dot{V}_r \le \sum_{i=1}^{2} \varepsilon_{1i} \rho_{1i} + \rho_2 \varepsilon_2 - e^T Q e \tag{18}$$

For $\dot{V}_r < 0$, it is then sufficient that the quadratic term on e is large enough to overcome the positive contributions of the other terms. Since Q is positive-definite, this can be guaranteed by the following equation:

$$\|e\| > \sqrt{\frac{\sum_{i=1}^{2} \varepsilon_{1i} \rho_{1i} + \rho_2 \varepsilon_2}{\underline{\lambda}(Q)}} \triangleq r_u \tag{19}$$

where r_u represents the uub radius and $\underline{\lambda}(Q)$ is the smallest eigenvalue of Q. For the actuated joints, closed-loop trajectories will ultimately enter and remain on the smallest level set of V_r which contains a ball of radius r_u. The designer must adjust $\rho_{1i}, \rho_2, \varepsilon_{1i}, \varepsilon_2, \Lambda$, and Π to achieve an acceptable tradeoff between good tracking accuracy (decreasing r_u), while avoiding excessive control chattering (increasing r_u). Remarks:

(1) Although damping was considered for the actuated joints through matrix B_a, the stability proof does not require it. Its presence can help reduce control effort, however.
(2) The regressors are functions of actuated joint positions and velocities only, assumed to be available as real-time measurements. An estimate of the unactuated acceleration can be obtained by online numerical differentiation, and a bound for the acceleration estimation error can be obtained according to the differentiation method. A simpler approach is to use a zero estimate for the acceleration and set the error bound to the maximum knee acceleration that can be reasonably expected during prosthesis operation. This eliminates the need for acceleration estimation altogether.
(3) Splitting the regressor along individual actuated coordinates allows us to use separate gains ρ_{1i} whose magnitudes are tailored to those of the corresponding parameters and regressors. If this is not done, a conflict may arise in practice, when tuning the value of a single ρ. Indeed, ρ may need to be increased so that sufficiently accurate tracking is obtained in some coordinates. At the same time, ρ may need to be reduced to avoid excessive chattering in control channels which are already achieving good tracking.
(4) The regressors and corresponding parameters for the passive leg prosthesis have been listed in the Appendix, along with the bound for $\|M_{12}\|$.

The designer must tune $\Pi, \Lambda_i, \rho_{i1}, \rho_2$, and the ε constants. The first matrix increases the damping effect on the actuated joints, the second accelerates the convergence of the tracking error and the remaining gains are used to guarantee robustness against parametric uncertainty. Note that boundedness of the unactuated coordinate follows from rearranging Eq. (6) as follows:

$$M_{22}\ddot{q}_u + C_{22}\dot{q}_u + R(\dot{q}_u, q_u) + g_u = -(M_{21}\ddot{q}_a + C_{21}\dot{q}_a + F_u) \tag{20}$$

Since tracking of $q_a^d(t)$ is achieved with bounded errors, q_a and its derivatives must be bounded. Matrices M_{21} and C_{21} are themselves bounded, and so is F_u. Therefore, the term on the right-hand side of Eq. (20) acts as a bounded input to the unactuated coordinate. Equation (20) represents the dynamics of a passive mechanical system driven by a bounded input. Its position and velocity states must then remain bounded.

3.1 Simulation. A simulation was conducted for the robust passivity-based controller (RPBC) under motion profile tracking. A set of reference profiles $q_1^d(t)$ and $q_2^d(t)$ were available from human motion studies. Their first two derivatives were computed offline by numerical differentiation and spline smoothing. The control tuning parameters used in this simulation were set to the best values found in subsequent real-time trials (Sec. 5). An intentional parametric mismatch in Θ between plant and controller was introduced to evaluate robustness. In particular, the controller used the nominal Θ_0, while the plant used $\Theta_0 + \Delta\Theta$, where the components of $\Delta\Theta$ were selected randomly from the interval $[-0.5\Theta_0,\ 0.5\Theta_0]$. Figure 4 shows the results, indicating that the controller is capable of achieving accurate tracking without exceeding amplifier saturation limits. Convergence of the Lyapunov function of Eq. (9) is also shown, although it increases its value during brief instants due to the nonideality of the deadzone implementation.

4 Independent-Joint Sliding Mode Control

A simple alternative to the coupled controller is to take advantage of the high transmission ratios between the motors and their driven links and treat the robot as a decoupled mechanical system. As shown in [9,10], the actuator-centric models have the form

$$J\ddot{\theta} + b\dot{\theta} = ku + \tau_d \tag{21}$$

where $\theta(t)$ is the controlled position variable, $u(t)$ is the control voltage (assumed proportional to motor torque), k is a constant reflecting a combination of servo amplifier gain, motor torque constant and rotary/linear motion conversion, J is the inertia of the load and motor, and b is a viscous damping coefficient. Variable τ_d represents an uncertain torque input consisting of external torque disturbances, unmodeled dynamics, parametric uncertainties, and unmodeled static effects, such as friction torque. Unmodeled dynamics include gravity torque and inertial coupling. SMC was chosen due to its good robustness properties and straightforward implementation [18,20,21]. In terms of the tracking error $e = \theta^d - \theta$, the system of Eq. (21) admits a sliding function of the form $s = \dot{e} + \lambda e$, with $\lambda > 0$ a tunable constant. Note that if $s(t) = 0$ for all t after some reaching time t_r, ideal first-order decay is achieved for the tracking error. An SMC law capable of achieving and maintaining $s = 0$ in finite time despite the presence of the uncertain term τ_d has the form

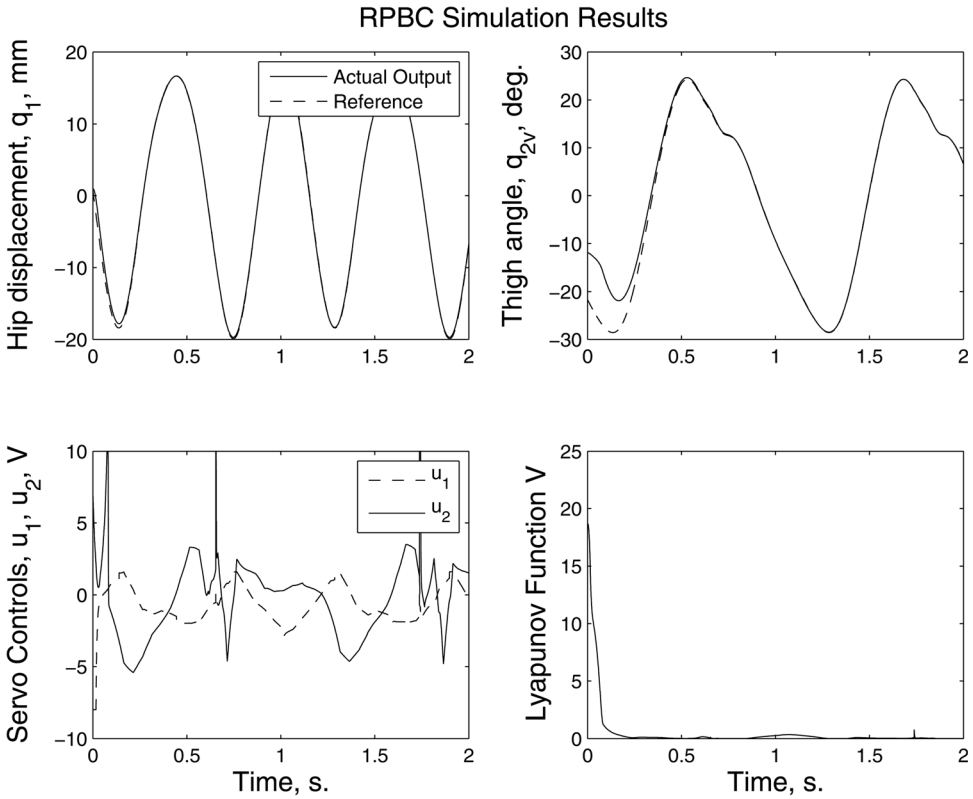

Fig. 4 Simulation of the RPBC in motion reference tracking with 50% parameter perturbation

$$u = \frac{J}{k}\left[(\ddot{\theta}^d + \lambda\dot{\theta}^d) + \left(\frac{b}{J} - \lambda\right)\dot{\theta} + \eta\,\mathrm{sign}\,(s)\right] \tag{22}$$

where $\eta > 0$ is chosen according to an assumed bound for τ_d. Note that motion profiles to be tracked and their derivatives enter the control law through the feedforward term $\ddot{\theta}^d + \lambda\dot{\theta}^d$. To limit chattering, a continuous approximation to the signum function is used, namely, a saturation function. Implementation of this control law is simpler than that of a PID controller, since no *online* integration or differentiation are needed, and only position and velocity measurements are required, which are available from optical encoders. Figure 5 shows a simulation of the IJSMC to the robot and prosthesis model. In this simulation, point contact between the prosthesis endpoint and the treadmill is assumed. A treadmill belt compliance for vertical deflections is taken from experimental measurements, and vertical ground reaction is calculated from Z_{LC} shown in the Appendix. It can be seen that accurate tracking is achieved and that the sliding functions converge to and remain within their boundary layers.

5 Real-Time Control Tests

The purpose of the tests is twofold: to demonstrate the validity of the passivity-based controller developed in this paper and to compare it with the IJ-SMC. Tests were conducted under pure motion tracking mode, and were initiated without ground contact. Then, manual biasing of the vertical stage was used to gradually "land" the foot on the treadmill, monitoring the force sensed by the foot-mounted strain gage. The speed of the treadmill was set to 2.6 miles per hour, the value at which the normal walk gait data were taken. The center of oscillation of the thigh was also biased manually once the foot was engaged in a swing-stance cycle. This was done so that overall motion resembled natural walking as much as possible, given the limitations associated with a passive prosthesis. Achievement of natural motion was judged quantitatively by achieving a ground reaction magnitude and a knee angle variation which matched human data for the hip and thigh motion profiles being tracked. Natural gait was judged qualitatively by ensuring that the stance phase was initiated with heel contact, transitioning to forefoot contact, and without using excessive thigh angle biasing.

The Mauch MicroLite S knee was adjusted to a flexion setting of 7 and an extension setting of 2. Although manufacturer data are unavailable regarding the damping constants associated with these settings, custom measurements carried out by the authors provide estimated values of $b = 1.57$ N s/mm for flexion and $b = 0.533$ N s/mm for extension.

Controllers are compared on the basis of their tracking abilities under full loading conditions, considering the amount of chattering required to achieve a given tracking accuracy. Test conditions were maintained as similar as possible for both controllers, although some differences to be elaborated below were unavoidable due to manual biasing during the tests. Note that the thigh angle coordinate q_2 is measured relative to a horizontal reference in the robotic model; however, results are presented in terms of its complement q_{2v}, which is more commonly used in biomechanics studies.

5.1 Robust Passivity-Based Controller. Two tests were conducted: one with nominal Θ parameters arising from modeling and parameter estimation, and another one with an intentional random perturbation in each component of Θ with a deviation of up to 10%. The RPBC was initially tuned in simulation with satisfactory results. Although the initial simulation values led to stable motion, chattering was large and it was evident that tracking accuracy could be improved with online tuning. Final values of the gains were $\Lambda = \mathrm{diag}(80, 7.5)$; $\Pi = \mathrm{diag}(10, 0.1)$; $\rho_{11} = 140$; $\rho_{12} = 5$; $\varepsilon_{11} = 2$; $\varepsilon_{12} = 7$; $\rho_2 = 1$; and $\varepsilon_2 = 1$. Figure 6 shows the hip displacement and thigh angle tracking performance achieved by the RPBC, as well as the control voltage histories for the nominal case. Figure 7 shows the knee angle and reaction force

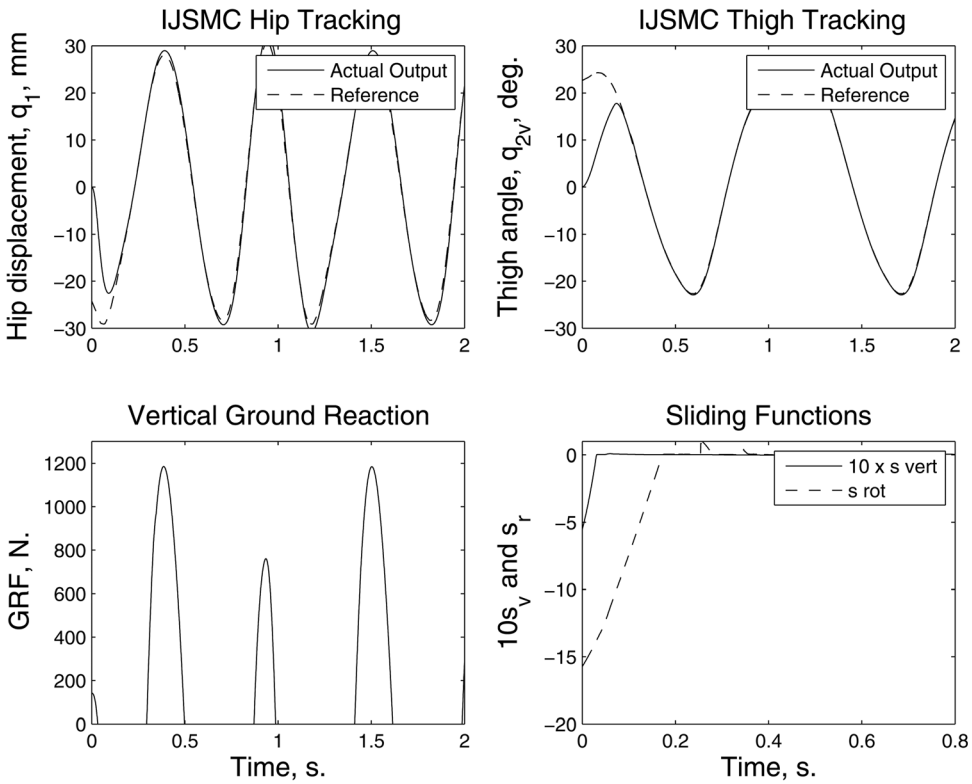

Fig. 5 Simulation of IJ-SMC

histories. During the real-time tests, manual biasing was applied until a force peak of 1000 N was observed. As expected, the ground forces act as disturbances preventing exact tracking of vertical hip displacement and thigh angle during ground contact. Although knee angle is not being controlled, the prosthesis mechanism maintains it between 0 and 70 deg, a range compatible with normal human walking at the test speed. Note also that the control voltages reach the amplifier saturation limits of ± 8 V for the

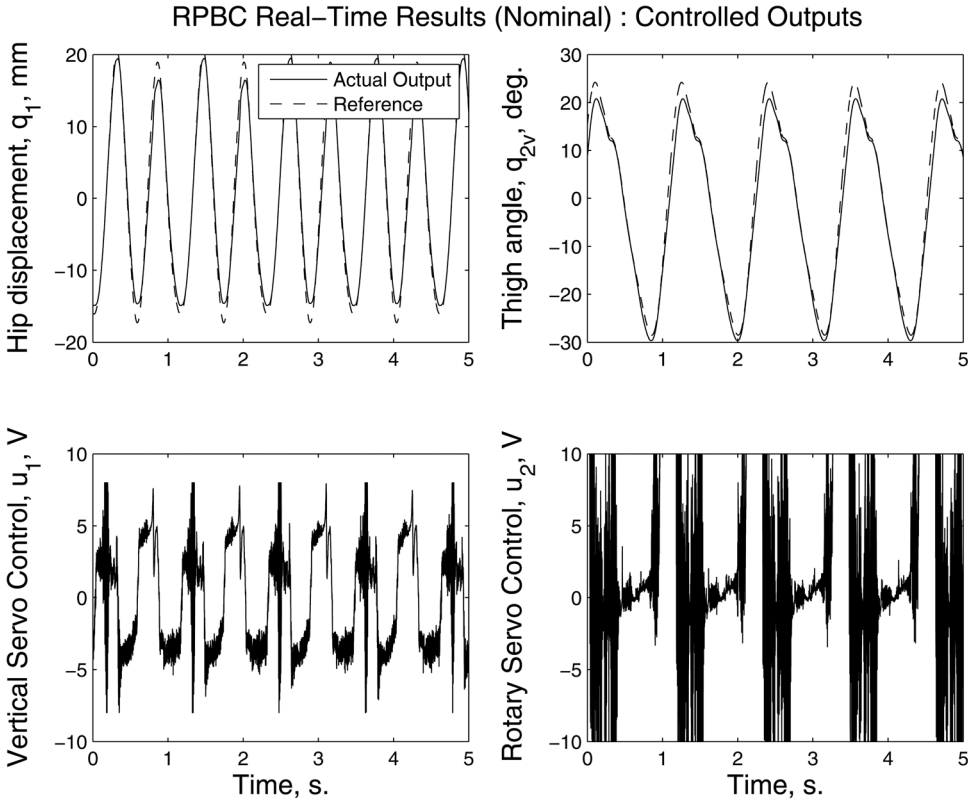

Fig. 6 RPBC: hip displacement and thigh angle tracking performance and control voltages (nominal)

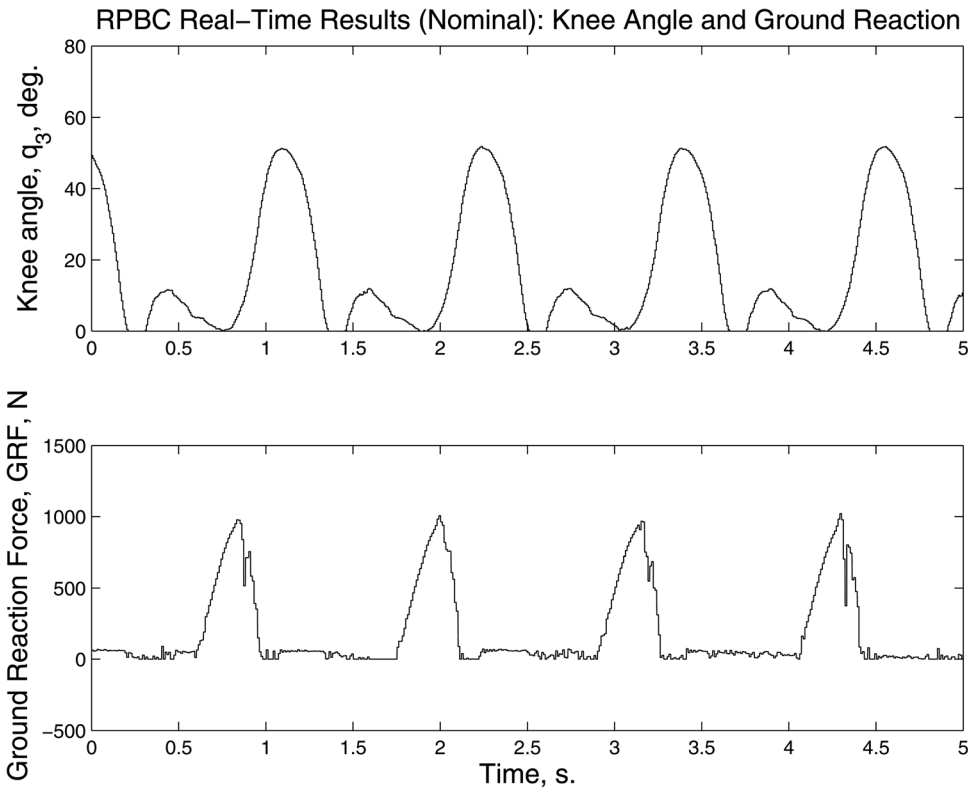

Fig. 7 RPBC: knee angle and vertical ground reaction force (nominal)

vertical stage and ±10 V for the rotary stage. The tracking results with RPBC and off-nominal plant parameters are shown in Fig. 8. Chattering in the respective control channels can be measured by the spectral energy above an arbitrary frequency. The fundamental frequency of the control inputs (i.e., the one correlated with the periodicity of the gait data) is 0.87 Hz. Fast Fourier transform (FFT) analysis reveals that the motion references do not contain significant frequency components beyond 10 Hz. Spectral

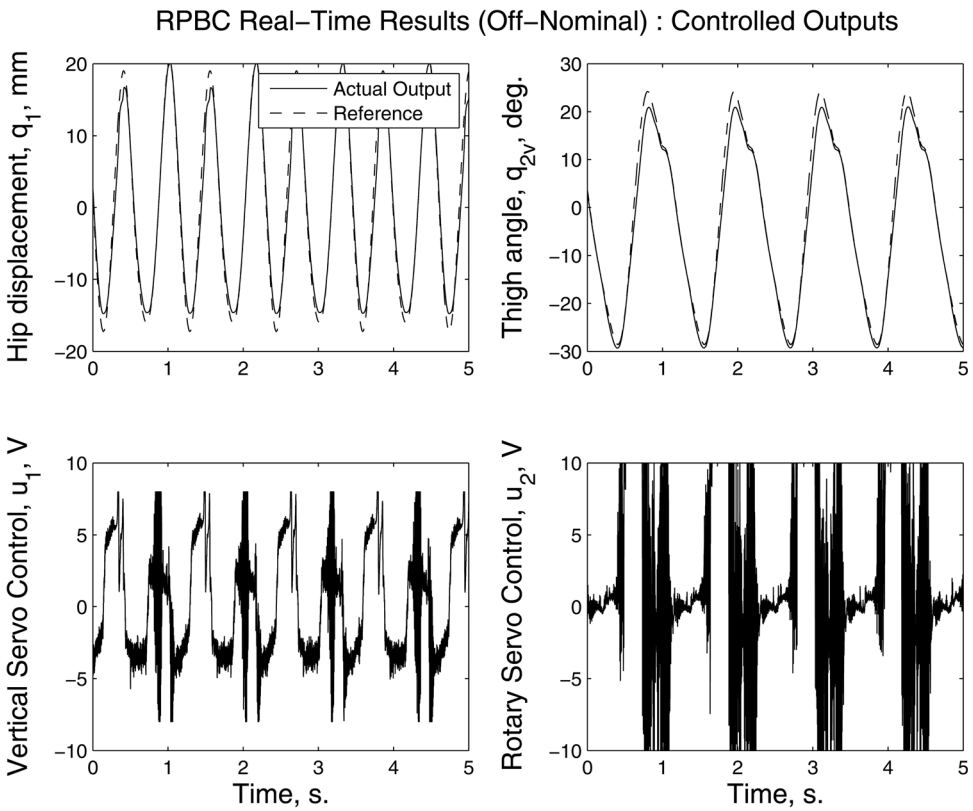

Fig. 8 RPBC: hip displacement and thigh angle tracking performance and control voltages (off-nominal)

Table 1 Summary of tracking performance and chattering measures

	$\tilde{q}_1$ rms	$\tilde{q}_2$ rms	u_1 chatter	u_2 chatter
RPBC nominal	1.64	2.61	7.39	22.9
SMC nominal	1.15	2.08	1.69	2.18
RPBC off-nominal	1.76	2.44	8.67	21.9
SMC off-nominal	1.03	1.93	1.31	2.16

energies found in the control signals above this frequency can be attributed to the control algorithm and electronics and can be reasonably used to compare control activity. The length of the data records and a sampling period of 5×10^{-4} s implies a frequency resolution of 0.2 Hz and an FFT frequency range of 1 kHz. A measure of chattering is obtained by an rms average of FFT magnitudes between 10 Hz and 1 kHz normalized by the length of the data record. Chattering levels according to this measure for the various tests are shown in Table 1, along with tracking performance data.

5.2 Independent-Joint Sliding Mode Controller. Decoupled control laws of the form of Eq. (22) were used for the vertical and rotary servos. Servo system constants were obtained by system identification and custom measurements [9,10] as $J_1 = 1$ kg m^2, $b_1 = 44.4$ N m s, and $k_1 = 1610$ N m/V for the vertical system as $J_2 = 1$ kg m^2, $b_2 = 6.5$ N m s, and $k_2 = 10$ N m/V for the rotary system. Sliding mode control parameters for the vertical servo system were chosen as $\eta_1 = 10^4$; $\lambda_1 = 90$; and $\phi_1 = 166$. The corresponding parameters for the rotary servo system were $\eta_2 = 50$; $\lambda_2 = 10$; and $\phi_2 = 0.5$.

Figure 9 shows the tracking performance and control input histories for the same motion references as used with the RPBC. The tracking accuracy is given by the rms errors of 2.28 mm for q_1 and 2.15 deg for q_{2v}. The chattering levels for u_1 and u_2 are 8.52 V and 6.70 V, respectively, calculated as described for the RPBC. It is observed that the control inputs do not reach amplifier saturation levels. Figure 10 shows the knee angle and vertical ground reaction force. Vertical biasing was used to achieve a force peak of 1000 N, and the thigh angle was manually biased during operation to obtain the initial heel strike indicative of a normal gait pattern. As with RPBC, a test was conducted using an intentional 10% perturbation in plant parameters used by the controller (b, J, and k for each channel). Tracking results for this case are shown in Fig. 11.

5.3 Discussion. Both controllers achieved rms tracking errors of 1.75 mm or less for vertical hip displacement (4.6% of the motion reference range) and 2.6 deg or less for thigh swing (5.5% of the motion reference range). Chattering measures were significant larger for u_2 when using RPBC. Table 1 summarizes the results. Two observations are in order in regard to Table 1. First, tracking performance and chattering levels are essentially maintained when plant parameters are intentionally perturbed. Second, chattering levels in u_2 are significantly higher for RPBC regardless of nominal or off-nominal conditions, but this does not occur in simulation studies, even when large parameter perturbations are introduced. Therefore, excessive chattering is attributed to effects present in the real system that were not modeled. We were able to trace the source of chattering to backlash in the thigh rotation gear mechanism. The vertical positioning mechanism uses a ballscrew which is essentially backlash-free, which explains the absence of chattering in u_1. Although backlash is present in the system regardless of control strategy, significantly smaller chattering levels were observed in u_2 when using IJ-SMC. This is because RPBC implements an approximate model inversion through Eq. (10), which includes the actuator models and the coupled dynamics of the robotic links. Since the actuator models do not include backlash, a significant mismatch occurs between actual and modeled plant behavior, particularly at the times when the

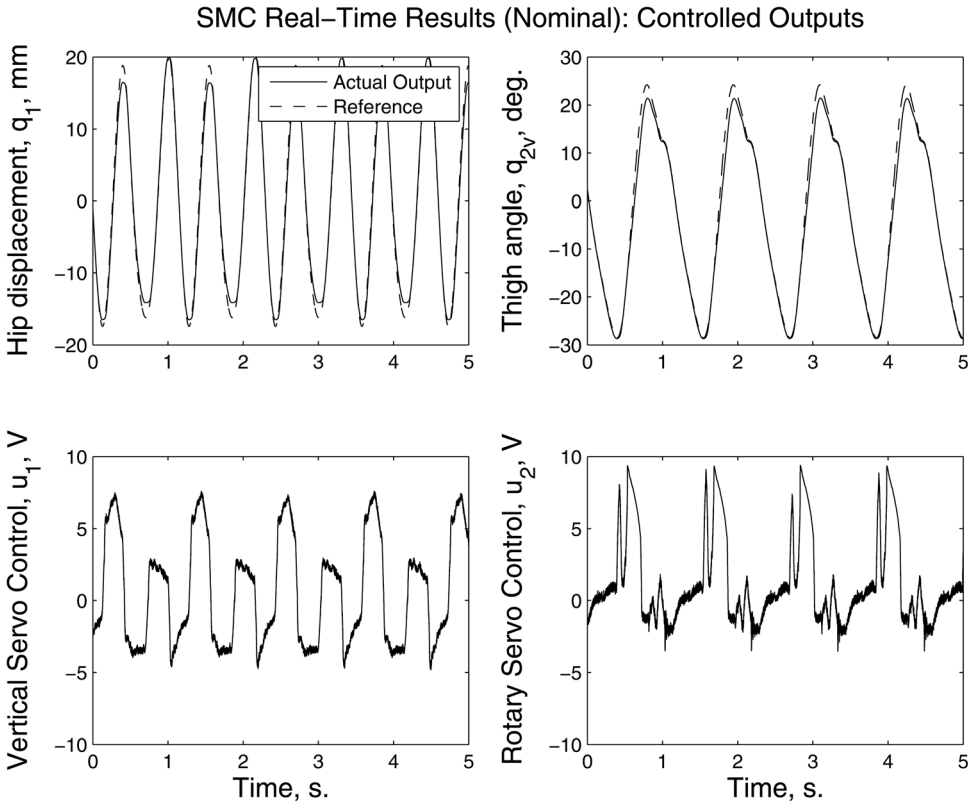

Fig. 9 IJ-SMC: hip displacement and thigh angle tracking performance and control voltages (nominal)

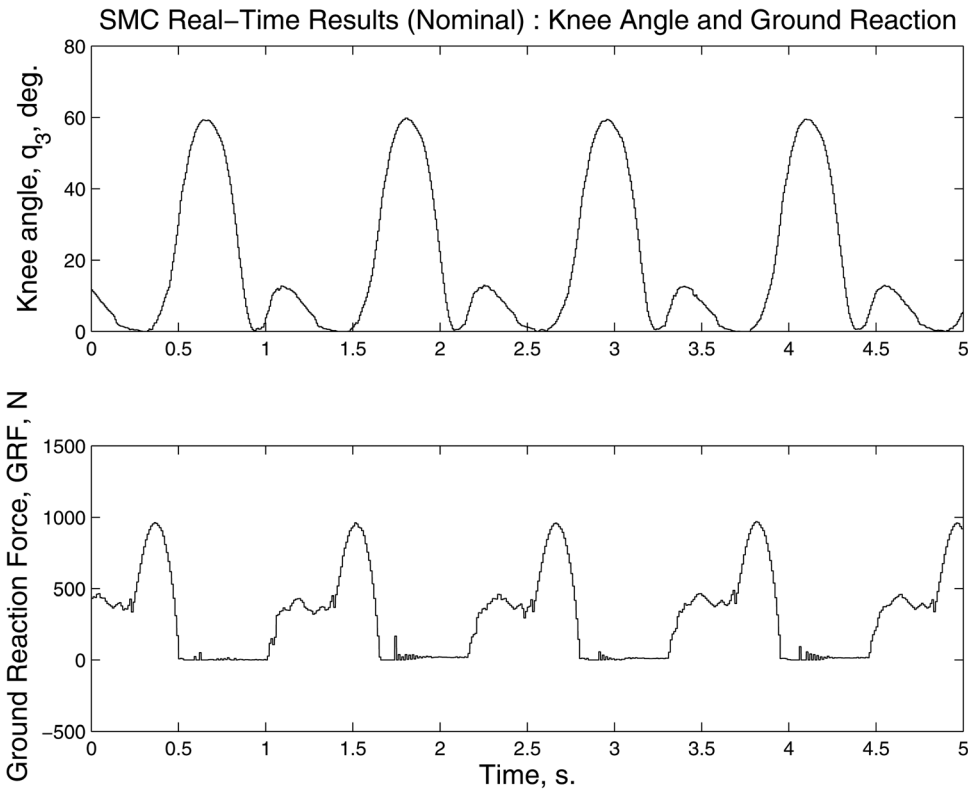

Fig. 10 IJ-SMC: knee angle and vertical ground reaction force (nominal)

gears become disengaged. Unlike errors due to parametric uncertainty, backlash (or other nonlinearity) are not explicitly addressed by RPBC. In contrast, the approximate model inversion used in the IJ-SMC law of Eq. (22) contains only actuator dynamics up to the driving gear, treating inertial coupling among links, friction and other effects as a disturbance. Model inversion is more accurate in this case, since actuator dynamics were determined accurately by system identification. This explanation can be

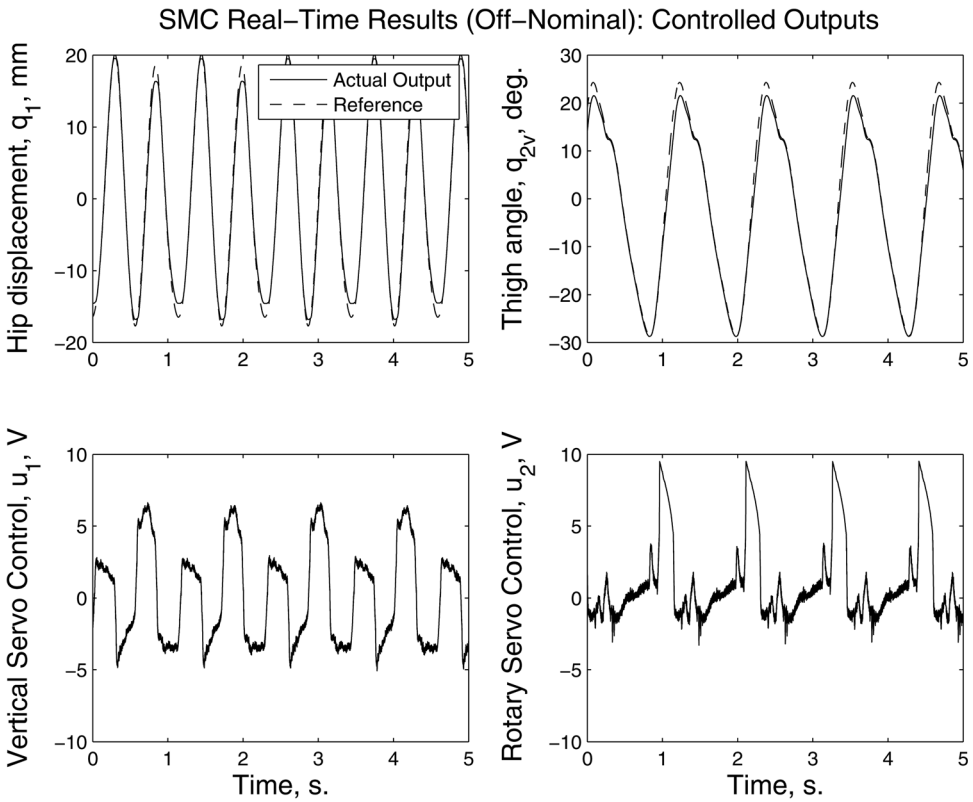

Fig. 11 IJ-SMC hip displacement and thigh angle tracking performance and control voltages (off-nominal)

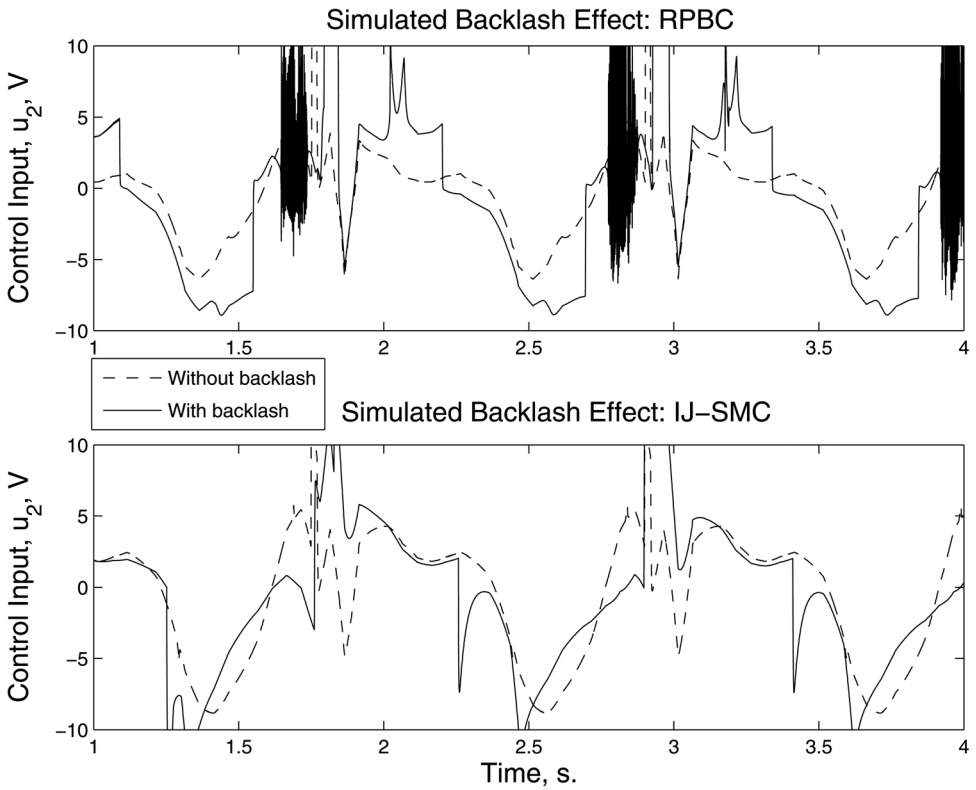

Fig. 12 Simulation of backlash effects: RPBC versus IJ-SMC

confirmed in simulation by introducing a backlash element in the thigh rotation drivetrain and testing each controller. We were able to reproduce the same effect in simulation: chattering due to backlash is higher when using RPBC. Figure 12 shows the simulated u_2 with each controller. Note that chattering has been identified as problematic in similar passivity-based implementations [22]. Another reason for the higher chattering levels found with RPBC is that the "nominal" values of Θ come from measurements which are subject to errors and should not be regarded as "true" parameters. The difference between nominal and actual parameters must be overcome with high values of the switching gains ρ during online tuning, giving rise to chattering. IJ-SMC relies on only six actuator parameters which exclude highly uncertain quantities, such as friction coefficient, link inertias, and center-of-gravity locations. RPBC, in contrast, requires a complete dynamic model and nine independent parameter estimates. Note that although extensive online tuning was conducted with each controller to achieve good performance, the numerical values of rms tracking error and chattering measure are tailored to this particular set of gains.

The observed ability of the IJ-SMC to offer good performance is due to the high transmission ratios used in each servo. Indeed, inertial coupling among links and gravity forces appear at the motor shaft after division by the square of the gear ratio. Thus, the servos operate practically in a decoupled mode. In this situation, the simplicity of the IJ-SMC (only three adjustable control parameters per channel) represents an advantage over the RPBC, which has five adjustable control parameters per channel, making tuning more difficult.

Although the peak magnitude of the ground reaction matched the RPBC case, its shape is different. This is due to the fact that the prosthesis is not actuated at the knee. This means that the trajectories exhibited by uncontrolled variables, such as knee angle or ground reaction, are highly influenced by the orientation and velocity of the foot at the strike instant. In turn, these two variables depend on how manual biasing is used. This difference does not prevent a meaningful comparison of controllers in terms of their tracking accuracy against the amount of chattering required.

The RPBC has the advantage of having guaranteed robust stability, backed by theoretical Lyapunov analysis. To the extent of the authors' knowledge, there is no proof available that an independent-joint sliding mode controller (without gravity compensation) achieves asymptotic tracking of the actuated coordinates while maintaining the unactuated coordinates bounded.

6 Conclusions

A robust controller for motion tracking was developed by suitably extending the passivity-based robot control technique to account for the lack of actuation at the knee joint and to facilitate tuning. The developed controller was compared with a simple, decoupled sliding mode controller. Good tracking of hip displacement and thigh angle normal walk motion profiles was achieved with both controllers, even during ground contact, where large disturbance forces were applied. In our tests, the passivity-based controller exhibited higher chattering in the thigh rotation control channel for the same tracking accuracy. We were able to trace this effect to backlash in the thigh rotation drive train. Modeling, control development, and real-time operation were conducted with a passive leg prosthesis. For prostheses which produce knee torque by means other than passive damping, an appropriate model must be used and the controller redesigned. Also, when actively damped or powered knee prosthesis is tested using this robot, the passivity-based approach may prove more useful than decoupled control due to the availability of a systematic theoretical framework from where to derive control laws with guaranteed stability and robustness. The higher sensitivity of RPBC to backlash motivates further research into the subject.

Although a motion control approach was adopted in this work, other test modalities are possible. For instance, a mixed motion/force approach may be used, where motion control is still used for both degrees of freedom in the swing phase and for thigh angle in

the stance phase, but hip displacement is controlled in the stance phase so that a desired ground force profile is tracked. Also, with actively damped or powered knees, an impedance synthesis approach may be undertaken, where control is used to track hip and thigh motions while controlling the knee actuator to replicate the moment/velocity impedance observed in human knees.

Acknowledgment

This work was supported by the State of Ohio, Department of Development and Third Frontier Commission, which provided funding through the Cleveland Clinic in support of the project Rapid Rehabilitation and Return to Function for Amputee Soldiers.

Appendix

Vertical coordinate of the point of application of the ground reaction (point-foot model)

$$Z_{\mathrm{LC}} = q_1 - l_{cy}\cos(q_2+q_3) + (c_3+l_{cx})\sin(q_2+q_3) + l_2\sin(q_2) \tag{A1}$$

External force Jacobian at point of application

$$\begin{aligned}
J_{\mathrm{e}}(1,1) &= 0\\
J_{\mathrm{e}}(1,2) &= -(c_3+l_{cx})\sin(q_2+q_3) + l_{cy}\cos(q_2+q_3) - l_2\sin(q_2)\\
J_{\mathrm{e}}(1,3) &= -(c_3+l_{cx})\sin(q_2+q_3) + l_{cy}\cos(q_2+q_3)\\
J_{\mathrm{e}}(2,1) &= J_{\mathrm{e}}(2,2) = J_{\mathrm{e}}(2,3) = 0\\
J_{\mathrm{e}}(3,1) &= 1\\
J_{\mathrm{e}}(3,2) &= (c_3+l_{cx})\cos(q_2+q_3) + l_{cy}\sin(q_2+q_3) + l_2\cos(q_2)\\
J_{\mathrm{e}}(3,3) &= (c_3+l_{cx})\cos(q_2+q_3) + l_{cy}\sin(q_2+q_3)
\end{aligned}$$

Regressors and parameter vectors

$$\begin{aligned}
Y_1(1) &= a_1\\
Y_1(2) &= a_1 - g\\
Y_1(3) &= a_2\cos(q_2) - \dot{q}_2 v_2\sin(q_2)\\
Y_1(4) &= a_2\cos(q_2+q_3) - v_3(\dot{q}_2\sin(q_2+q_3) + \dot{q}_3\sin(q_2+q_3))\\
&\quad - v_2(\dot{q}_2\sin(q_2+q_3) + \dot{q}_3\sin(q_2+q_3)) + a_3\cos(q_2+q_3)\\
Y_1(5) &= \mathrm{sign}(q_1)\\
Y_2(1) &= a_1\cos(q_2) - g\cos(q_2)\\
Y_2(2) &= a_1\cos(q_2+q_3) - g\cos(q_2+q_3)\\
Y_2(3) &= a_2\\
Y_2(4) &= 2a_2\cos(q_3) + a_3\cos(q_3) - v_3(\dot{q}_2\sin(q_3) + \dot{q}_3\sin(q_3))\\
&\quad + \dot{q}_3 v_2\sin(q_3)\\
Y_2(5) &= a_3\\
Y_2(6) &= \dot{q}_2
\end{aligned}$$

where a_i and v_i are the entries of vectors a and v.

Parameter vectors

$$\Theta_1 = \begin{bmatrix} m_0 \\ m_1+m_2+m_3 \\ m_2(c_2+l_2)+m_3 l_2 \\ m_3 c_3 \\ f \end{bmatrix}$$

$$\Theta_2 = \begin{bmatrix} m_2(c_2+l_2)+m_3 l_2 \\ m_3 c_3 \\ I_{2z}+I_{3z}+J_{\mathrm{m}}r^2+c_2^2 m_2+c_3^2 m_3+l_2^2 m_2+l_2^2 m_3+2c_2 l_2 m_2 \\ l_2 c_3 m_3 \\ I_{3z}+m_3 c_3^2 \\ b \end{bmatrix}$$

See Refs. [9,10] for the definition of inertial parameters.

Bound on $\|M_{12}\|$

$$\begin{aligned}
M_{12} &= \begin{bmatrix} m_3 c_3\cos(q_2+q_3) \\ m_3 c_3^2 + l_2 m_3 c_3\cos(q_3) + I_{3z} \end{bmatrix}\\
&= \begin{bmatrix} \Theta_2(2)\cos(q_2+q_3) \\ \Theta_2(5) + \Theta_2(4)\cos(q_3) \end{bmatrix}
\end{aligned}$$

Using the Euclidean norm $\|M_{12}\|^2 \le \Theta_2^2(2) + (\Theta_2(5)+\Theta_2(4))^2$.

References

[1] Laferrier, J., and Gailey, R., 2010, "Advances in Lower-Limb Prosthetic Technology," J. Phys. Med. Rehabil. Clin. North Am., **21**(1), pp. 87–110.

[2] Bellmann, M., Schmalz, T., and Blumentritt, S., 2010, "Comparative Biomechanical Analysis of Current Microprocessor-Controlled Prosthetic Knee Joints," Arch. Phys. Med. Rehabil., **91**(4), pp. 644–52.

[3] Chin, T., Machida, K., Sawamura, S., Shiba, R., Oyabu, H., Nagakura, Y., Takase, I., and Nakagawa, A., 2006, "Comparison of Different Microprocessor Controlled Knee Joints on the Energy Consumption During Walking in Trans-Femoral Amputees: Intelligent Knee Prosthesis (IP) Versus C-Leg," Prosthet. Orthot. Int., **30**(1), pp. 73–80.

[4] Johansson, J., Sherrill, D. M., Riley, P. O., Bonato, P., and Herr, H., 2005, "A Clinical Comparison of Variable-Damping and Mechanically Passive Prosthetic Knee Devices," Am. J. Phys. Med. Rehabil., **84**(8), pp. 563–75.

[5] Segal, A. D., Orendurff, M. S., Klute, G. K., McDowell, M. L., Pecoraro, J. A., Shofer, J., and Czerniecki, J. M., 2006, "Kinematic and Kinetic Comparisons of Transfemoral Amputee Gait Using C-Leg and Mauch SNS Prosthetic Knees," J. Rehabil. Res. Dev., **43**(7), pp. 857–70.

[6] Seroussi, R. E., Gitter, A., Czerniecki, J. M., and Weaver, K., 1996, "Mechanical Work Adaptations of Above-Knee Amputee Ambulation," Arch. Phys. Med. Rehabil., **77**(11), pp. 1209–1214.

[7] "Biomechatronische Systeme," 2013, Fraunhofer Institute for Manufacturing Engineering and Automation, Orthopaedics and Motion Systems, Stuttgart, retrieved on November 2013, http://ipa.fraunhofer.de/Orthopaedics_and_Motion_Systems.83.0.html?&L=2

[8] "Medical Device Solutions–Services," 2013, Cleveland Clinic Lerner Research Institute, Neuromusculoskeletal Simulator, retrieved on November 2013, http://mds.clevelandclinic.org/Services/BioRobotics/Services.aspx

[9] Richter, H., Simon, D., Smith, W., and Samorezov, S., 2012, "Dynamic Modeling, Parameter Estimation and Control of a Leg Prosthesis Test Robot," Appl. Math. Modell. (submitted).

[10] Richter, H., Simon, D., Smith, W. A., and Samorezov, S., 2013, "Dynamic Modeling and Parameter Estimation of a Leg Prosthesis Test Robot," Laboratory Report, retrieved on November 2013, http://academic.csuohio.edu/richter_h/lab/ccfrobot/

[11] Kwan, C., 1995, "Hybrid Force/Position Control for Manipulators With Motor Dynamics Using a Sliding-Adaptive Approach," IEEE Trans. Autom. Control, **40**(5), pp. 963–968.

[12] Wren, J., and Kreutz-Delgado, K., 1992, "Motion and Force Control of Multiple Robotic Manipulators," Automatica, **28**(4), pp. 729–743.

[13] Hogan, N., 1985, "Impedance Control: An Approach to Manipulation: Part II—Implementation," ASME J. Dyn. Syst., Meas., Control, **107**(1), pp. 8–16.

[14] Michael, J., 1999, "Modern Prosthetic Knee Mechanisms," Clin. Orthop. Relat. Res., **361**(47), pp. 39–47.

[15] van den Bogert, A., Samorezov, S., Davis, B., and Smith, W., 2012, "Modeling and Optimal Control of an Energy-Storing Prosthetic Knee," ASME J. Biomech. Eng., **134**(5), p. 051007.

[16] Spong, M., Hutchinson, S., and Vidyasagar, M., 2006, *Robot Modeling and Control*, Wiley, New York.

[17] Denavit, J., and Hartenberg, R., 1955, "A Kinematic Notation for Lower-Pair Mechanisms Based on Matrices," ASME J. Appl. Mech., **22**(2), pp. 215–221.

[18] Utkin, V., 1992, *Sliding Modes in Control Optimization*, Springer-Verlag, Berlin.

[19] Corless, M., and Leitman, G., 1981, "Continuous State Feedback Guaranteeing Uniform Ultimate Boundedness for Uncertain Dynamic Systems," IEEE Trans. Autom. Control, **26**(5), pp. 1139–1144.

[20] Edwards, C., and Spurgeon, S., 1998, *Sliding Mode Control: Theory and Applications*, Taylor and Francis, London.

[21] Slotine, J., and Li, W., 1990, *Applied Nonlinear Control*, Prentice Hall, Englewood Cliffs, NJ.

[22] Sage, H., De Mathelin, M., and Ostertag, E., 1999, "Robust Control of Robotic Manipulators: A Survey," Int. J. Control, **72**(16), pp. 1498–1522.